PCCP

PAPER

View Article Online
View Journal | View Issue

Cite this: *Phys. Chem. Chem. Phys.*, 2014, **16**, 12057

Computational investigation of structural and electronic properties of aqueous interfaces of GaN, ZnO, and a GaN/ZnO alloy†

Neerav Kharche,*[a] Mark S. Hybertsen*[b] and James T. Muckerman*[a]

Received 31st January 2014,
Accepted 24th March 2014

DOI: 10.1039/c4cp00486h

www.rsc.org/pccp

The GaN/ZnO alloy functions as a visible-light photocatalyst for splitting water into hydrogen and oxygen. As a first step toward understanding the mechanism and energetics of water-splitting reactions, we investigate the microscopic structure of the aqueous interfaces of the GaN/ZnO alloy and compare them with the aqueous interfaces of pure GaN and ZnO. Specifically, we have studied the $(10\bar{1}0)$ surface of GaN and ZnO and the $(10\bar{1}0)$ and $(1\bar{2}10)$ surfaces of the 1 : 1 GaN/ZnO alloy. The calculations are carried out using first-principles density functional theory based molecular dynamics (DFT-MD). The structure of water within a 3 Å distance from the semiconductor surface is significantly altered by the acid/base chemistry of the aqueous interface. Water adsorption on all surfaces is substantially dissociative such that the surface anions (N or O) act as bases accepting protons from dissociated water molecules while the corresponding hydroxide ions bond with surface cations (Ga or Zn). Additionally, the hard-wall interface presented by the semiconductor imparts ripples in the density of water. Beyond a 3 Å distance from the semiconductor surface, water exhibits a bulk-like hydrogen bond network and oxygen–oxygen radial distribution function. Taken together, these characteristics represent the resting (or "dark") state of the catalytic interface. The electronic structure analysis of the aqueous GaN/ZnO interface suggests that the photogenerated holes may get trapped on interface species other than the adsorbed OH^- ions. This suggests additional dynamical steps in the water oxidation process.

1. Introduction

Splitting water into hydrogen and oxygen using semiconductor-based heterogeneous photocatalysis plays a key role in a promising path to clean and sustainable energy production.[1] Pure GaN can catalyze water splitting; however, it is active only under UV irradiation owing to its large band gap (3.4 eV).[2,3] Domen's group has reported that the band gap of GaN can be reduced from the UV to the visible range by alloying it with ZnO.[4] The resulting band-gap-narrowed semiconductor GaN/ZnO alloy has been shown to be an efficient photocatalyst under visible light irradiation,[4] although the structure of its aqueous interface is not well understood. The microscopic structure of the aqueous interface is crucial in determining the electrostatics and the redox level alignment at the aqueous semiconductor interface.[5] Additionally, the mechanism of photocatalytic reactions critically depends on various local structural motifs, including the hydrogen bond network at the aqueous semiconductor interface.[6,7]

In this work, we use density functional theory based molecular dynamics (DFT-MD), to investigate the microscopic structural and electronic properties of aqueous interfaces of representative GaN/ZnO alloy structures and compare them with aqueous interfaces of GaN and ZnO. Most of the water splitting experiments are carried out using a GaN/ZnO photocatalyst in powdered form having a wurtzite crystal structure, however, it is not known which surfaces are photocatalytically active.[4,8] A recent experiment on high quality GaN nanowires grown using molecular beam epitaxy (MBE) has found that the non-polar $(10\bar{1}0)$ surface shows much higher photocatalytic activity compared to polar surfaces.[3] Therefore we have used the non-polar wurtzite $(10\bar{1}0)$ *m*- and $(1\bar{2}10)$ *a*-planes as model surfaces in our computational study. More specifically, we have studied the $(10\bar{1}0)$ surface of GaN and ZnO, and the $(10\bar{1}0)$ and $(1\bar{2}10)$ surfaces of the 1 : 1 GaN/ZnO alloy.

[a] *Chemistry Department, Brookhaven National Laboratory, Upton, New York 11973-5000, USA. E-mail: nkharche@bnl.gov, muckerma@bnl.gov*
[b] *Center for Functional Nanomaterials, Brookhaven National Laboratory, Upton, New York 11973-5000, USA. E-mail: mhyberts@bnl.gov*

† Electronic supplementary information (ESI) available: (1) Optimized water dimer geometries, (2) MP2 and CCSD(T) potential energy curves for water dimer, (3) bulk water diffusivity and system size effects, (4) optimized lattice parameters for bulk GaN and ZnO, (5) radial distribution functions of surface cations with O atoms in OH^- ions and water molecules, (6) spatial dependence of water structure at aqueous interfaces of GaN$(10\bar{1}0)$, ZnO$(10\bar{1}0)$, and GaN/ZnO$(1\bar{2}10)$ surfaces. See DOI: 10.1039/c4cp00486h

Knowledge of the structure of the GaN/ZnO alloy has evolved over the past several years.[9–20] Our first systematic theoretical study[9] employed the special quasirandom structures (SQS) method[21] to generate candidate disordered structures, and the candidate structure at each composition with the lowest energy was taken to be representative of that composition. The exception was for the 1:1 alloy, for which a more ordered structure than those generated by the SQS method was found to have a lower energy.[20] As pointed out by Wang and Wang, local order can significantly influence the degree of band gap reduction.[11] It was later found in a combined cluster expansion/Monte Carlo study based on DFT calculations[10] that the 1:1 alloy is unique, having a perfectly layered structure as its only stable low-temperature phase, but having a band gap of *ca.* 3.1 eV, making it uninteresting as a photocatalyst. The same Monte Carlo study predicted that the high-temperature phase (>870 °C) is predominantly disordered, but exhibits strong short-range order up to 2nd-nearest-neighbor interactions. In the present study, we employ a sample taken from the disordered phase from the 1:1 Monte Carlo simulation (reflecting the high-temperature synthesis conditions) that contains an equal number of Ga, N, Zn and O atoms to represent the 1:1 alloy.

Turning to the interface with water, very little is known at the atomic scale. With the possibility of important interface reactions, such as water dissociation, it is desirable to tackle this problem with an approach that intrinsically includes the role of and changes in local electronic structure, while still allowing for sampling of the dynamics inherent to the liquid water. Here we chose to use DFT-MD. These simulations are computationally demanding and it is only in recent years that studies of selected semiconductor–water interfaces have emerged. For example, under ambient conditions, water adsorbs molecularly on the TiO_2 anatase (101)[22] and rutile (110)[23] surfaces, dissociatively on Si-terminated SiC(001),[24] oxygen-rich GaP and InP(001),[25] and GaN(10$\bar{1}$0)[7,26] surfaces, while mixed molecular and dissociative water adsorption is found on the ZnO(10$\bar{1}$0)[27] surface. Furthermore, with reference to the long-term interest in catalytic mechanisms, such simulations not only provide insight into possible reaction center motifs, they also give important guidance as to the role of "wet" water and a means to test more phenomenological solvation models, effects of which have not been taken into account in older studies.[28–31]

This work addresses two key questions: (i) how does the acid–base chemistry at the aqueous semiconductor interface affect the structure of liquid water, and (ii) how far does the perturbation of the water structure induced by the semiconductor surface extend into the liquid. The aqueous interface chemistry is found to profoundly affect the structure of water molecules in contact with the surface. Water adsorption is substantially dissociative such that the surface anions (N or O) act as bases accepting protons from dissociated water molecules while the corresponding hydroxide ions bond with surface cations (Ga or Zn). Beyond a 3 Å distance from the semiconductor surface, water exhibits a bulk-like hydrogen bond network and oxygen–oxygen radial distribution function. This property of the aqueous interface allows for the calculation of the redox level alignment using reasonably sized model systems as shown in our recent work.[32] Additionally, the MD simulations provide representative structural models of the aqueous interface for mechanistic studies of water splitting. The GaN/ZnO alloy is known to support catalytic sites for water oxidation while a separate co-catalyst is required for proton reduction.[4,8] Based on our earlier mechanistic studies of water oxidation at the GaN–water interface, we expect that a hole will localize on an adsorbed OH^- ion to initiate and propagate a sequence of four proton-coupled hole-transfer steps for the oxidation of water into oxygen.[7,33] In this paper, we also investigate the propensity of localization of the photogenerated holes on the adsorbed OH^- ions by analyzing the projected density of states (PDOS) of various surface species sampled in the MD simulations.

The remainder of this paper is organised as follows. The computational methods and model systems are described in Section 2. Section 3 presents the structural and electronic properties of the various aqueous interfaces obtained from MD simulations. Conclusions and future directions of this work are outlined in Section 4.

2. Computational methods and model systems

2.1. Computational details

The MD simulations are performed using the Vienna *ab initio* simulation package (VASP)[34–36] based on DFT with the projector augmented wave (PAW) method.[37] The 4s, 4p, and 3d electrons of Ga and Zn, and the 2s and 2p electrons of N and O are treated as valence electrons. Based on our prior experience, we have used the DFT + U method within the Dudarev formulation[38] with the on-site Coulomb interaction parameters U_{Ga} = 3.9 eV and U_{Zn} = 6.0 eV to correct the DFT underestimation of electron correlation of the Ga and Zn d-orbitals.[9] The Brillouin zone is sampled only at the Γ-point because all calculations presented here involve large supercells.

We have used the non-local vdW-DF functional proposed by Dion *et al.*[39] to include the long-range van der Waals (vdW) interactions, which were recently shown to be important to accurately model liquid water under ambient conditions.[40–43] The vdW-DF exchange correlation energy can be expressed as

$$E_{xc} = E_x^{GGA} + E_c^{LDA} + E_c^{nl}$$

where E_x^{GGA} is an exchange functional in the generalized gradient approximation (GGA), E_c^{LDA} is the local correlation energy in the local density approximation (LDA) and E_c^{nl} is the non-local correlation energy describing the vdW interaction.[39] We have tested two versions of the vdW-DF functional based on the choice of the GGA exchange functional: (i) PBE-vdW, obtained by using the PBE exchange functional[44] and (ii) optB88-vdW, obtained by using the optB88 exchange functional recently proposed by Klimes *et al.*[45]

All DFT-MD simulations are performed within the Born–Oppenheimer (BO) approximation using a Nose–Hoover thermostat and a Verlet integrator with a time step of 0.5 fs. Initial water

structures are obtained from classical MD simulations within a NVT ensemble with the TIP4P potential using the GROMACS simulation package.[46] Following standard practice, the deuterium mass is used for H atoms. All MD simulations are carried out for 15 to 30 ps. The basis set size (plane-wave cutoff energy) is determined by comparing DFT calculations of water dimers with highly accurate CCSD(T) calculations, which are performed using the Gaussian 09 code.[47] The MD simulation temperature is determined by comparing the oxygen–oxygen radial distribution function (RDF) calculated from MD simulation with that deduced from experiments at room temperature. We find that good agreement with experiments is achieved for a plane-wave cutoff of 600 eV and the slightly elevated MD simulation temperature of 350 K.

2.2 Water dimer

To further calibrate the choice of functional, and to help determine the plane-wave energy cutoff required, for accurate description of the interaction between water molecules, we consider representative water dimer configurations shown in the insets of Fig. 1. In the first configuration (Fig. 1a), the water molecules are hydrogen bonded, while in the second configuration (Fig. 1b), the water molecules are constrained in such a way that lone pairs of electrons on oxygen atoms point at each other resulting in a repulsive interaction. The geometry optimizations are carried out using the MP2 method with the large aug-cc-pVTZ basis set. These geometries are used in all additional calculations. Both the MP2 and CCSD(T) calculations were corrected for basis set superposition error (BSSE) and the resulting energies were extrapolated to the complete basis set (CBS) limit using the two point extrapolation scheme proposed in ref. 48. For the hydrogen-bonded scan, all other degrees of freedom are allowed to relax while keeping the distance between the two oxygen atoms (O1 and O4) fixed. This permits the nature of the hydrogen bonding to change at short distance (R_{O-O} between 2.5 and 2.6 Å, Fig. 1(a)), resulting in an abrupt wiggle in the potential curve. In the repulsive scan, the distance between the two oxygen atoms is fixed and the dihedral angles H2–O1–O4–H5 and H3–O1–O4–H6 held at 90 degrees while all the remaining degrees of freedom are allowed to relax. All optimized water dimer geometries are provided in the ESI.†

The MP2-optimized water dimer geometries are used to calculate the potential energy curves at the CCSD(T)/CBS level of theory. These potential energy curves are shown in Fig. 1. The MP2 and CCSD(T) results are found to be in excellent agreement as shown in Fig. S1 in the ESI.† To calibrate the DFT calculations using the vdW-DF functional against the CCSD(T) calculations, we gradually increase the plane-wave cutoff until smooth potential energy curves are obtained for the same MP2-optimized water dimer geometries. We find that the relatively high-energy cutoff of 600 eV is required to obtain smooth potential energy curves. The comparison between the vdW-DF and benchmark CCSD(T) potential energy curves is illustrated in Fig. 1. The optB88-vdW results are in excellent agreement (within 20 meV) with the CCSD(T) results, while the PBE-vdW functional significantly overbinds water dimers. These findings are consistent with previous studies performed using norm-conserving pseudopotentials and plane-wave basis sets.[41] Therefore we have carried out all MD simulations using the optB88-vdW functional.

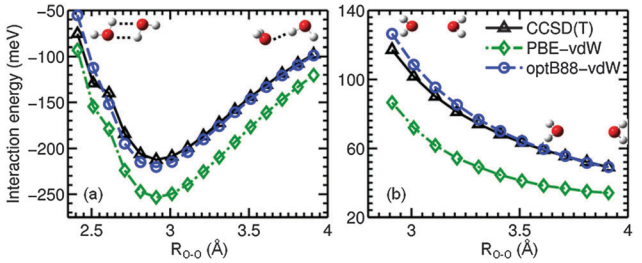

Fig. 1 Interaction energy of water dimer as a function of the separation between oxygen atoms. (a) Hydrogen bonded configuration. (b) Repulsive configuration.

2.3 Liquid water

It is now well established that the BO DFT-MD simulation of water at ambient conditions leads to significantly overstructured RDFs and lower diffusivity compared to experiments.[40–43,49,50] This discrepancy arises from the fact that the proton quantum effects are not included in the BO MD, which treats the nuclear motion classically. The quantum nature of nuclear motion can be approximately accounted for by increasing the MD simulation temperature. Higher simulation temperatures give softer RDFs and higher diffusivity in better agreement with experiments. In practice, the required simulation temperature is dependent on the exchange–correlation functional. To determine the required simulation temperature for the optB88-vdW functional, we use a reference system containing 32 water molecules in a cubic box of length 9.86 Å with periodic boundary conditions, which corresponds to the ambient density 1 g cm^{-3} of liquid water. The system is equilibrated for 5 ps followed by a 25 ps production run.

The oxygen–oxygen RDFs ($g_{OO}(r)$) calculated from the MD simulations at 325 K and 350 K are shown in Fig. 2 along with the experimental data at 298 K.[51] The liquid water simulated at 325 K is overstructured as seen from the taller peaks and deeper valleys in $g_{OO}(r)$ compared to the experimental result. The $g_{OO}(r)$ becomes softer with increasing temperature and the best agreement with experiments is obtained for 350 K. We analysed the hydrogen-bond network by calculating the number of hydrogen-bonds per water molecule. Two water molecules are considered hydrogen bonded when the O atoms are closer than 3.5 Å and the OHO angle is greater than 140°. The number of hydrogen bonds per water molecule decreases from 3.64 at 325 K to 3.54 at 350 K. We analysed the dynamical properties of the simulated water by means of the self-diffusion coefficient (D_0) calculated using established procedures employing the Einstein relation.[49,52–54] D_0 obtained from the 350 K simulation is found to agree reasonably well with the experimental data for heavy water (see ESI† for further details). Additionally, we have investigated the system-size dependence by comparing the 32 water molecule system with a larger system containing

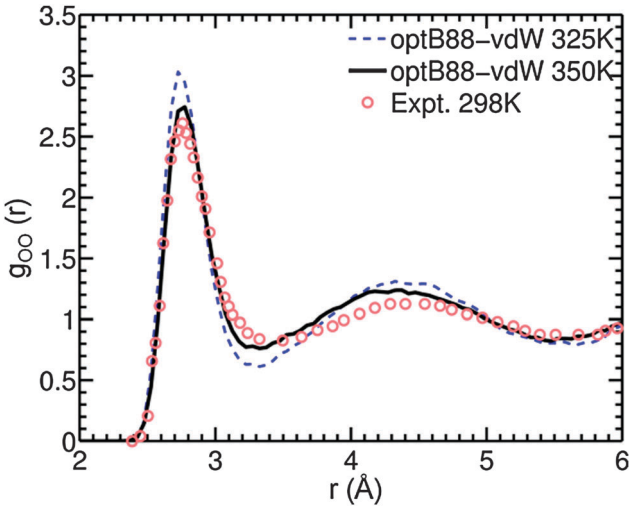

Fig. 2 Oxygen–oxygen radial distribution function calculated using optB88-vdW functional at the MD simulation temperatures of 325 K (dotted line) and 350 K (solid line). The experimental data[51] are shown by the hollow circles.

64 water molecules, and we do not find significant differences (further details are provided in the ESI†).

2.4 Semiconductor–water interface

We have studied the $(10\bar{1}0)$ surface of GaN, ZnO, and the 1 : 1 GaN/ZnO alloy and the $(1\bar{2}10)$ surface of the GaN/ZnO alloy. The structure of the aqueous interface of each surface is investigated using a DFT-MD simulation of a repeated orthorhombic supercell in which a semiconductor slab alternates with a water filled region as shown in Fig. 3. The slabs of pure GaN and ZnO (Fig. 3a and b) are constructed using the optimized lattice parameters obtained from DFT. The optimized lattice constants agree with the experimental values to within 1.3% (further details are provided in the ESI†). Our earlier studies using a DFT-based cluster expansion model and Monte Carlo simulations have found strong short-range order (SRO) in GaN/ZnO alloys.[10] A similar study by other authors has shown that the structural and electronic properties of a GaN/ZnO alloy with SRO are significantly different from the completely random alloy.[11] To include realistic SRO in the DFT-MD simulations, we cut GaN/ZnO slabs with 1 : 1 composition of GaN and ZnO (Fig. 3c and d) from a large 432 atom cell of composition $Ga_{0.5}Zn_{0.5}N_{0.5}O_{0.5}$ generated by a Monte Carlo simulation using the same cluster expansion model developed in ref. 10.

The dimensions (L_x, L_y, and L_z) of the supercells are given in Table 1. The lateral dimensions of the GaN and ZnO supercells are chosen based on the earlier studies of the structure of a water monolayer on GaN and ZnO surfaces. An adsorbed water monolayer forms (1×1) and (2×1) periodic structures on GaN$(10\bar{1}0)$ and ZnO$(10\bar{1}0)$ surfaces, respectively.[55,56] To adequately sample such structures in MD simulations, we have used GaN and ZnO supercells of sizes 3×2 and 4×2, respectively. The atom-type disorder on GaN/ZnO alloy surfaces is expected to prevent the formation of ordered structures in the adsorbed water layer. We have used $(10\bar{1}0)$ and $(1\bar{2}10)$ GaN/ZnO supercells of lateral dimensions comparable to the GaN and ZnO supercells. The thickness of semiconductor slabs ranges from 12.82 to 14.76 Å and it is sufficient to prevent interactions between adsorbed water molecules on the two sides of the slabs.

To obtain the initial structure of the dry surface, we relax the semiconductor slabs until the residual force on each atom is smaller than 0.02 eV $Å^{-1}$. All surfaces relax *via* the contraction of surface anion–cation bonds accompanied by out-of-plane displacement of anions, which is in agreement with the earlier studies on pure GaN and ZnO surfaces.[57,58] Next, a slab of water of density 1 g cm^{-3} with the same lateral dimensions as the semiconductor slab and thickness of about 15 Å is inserted between the surfaces in each supercell. The separation (t_z)

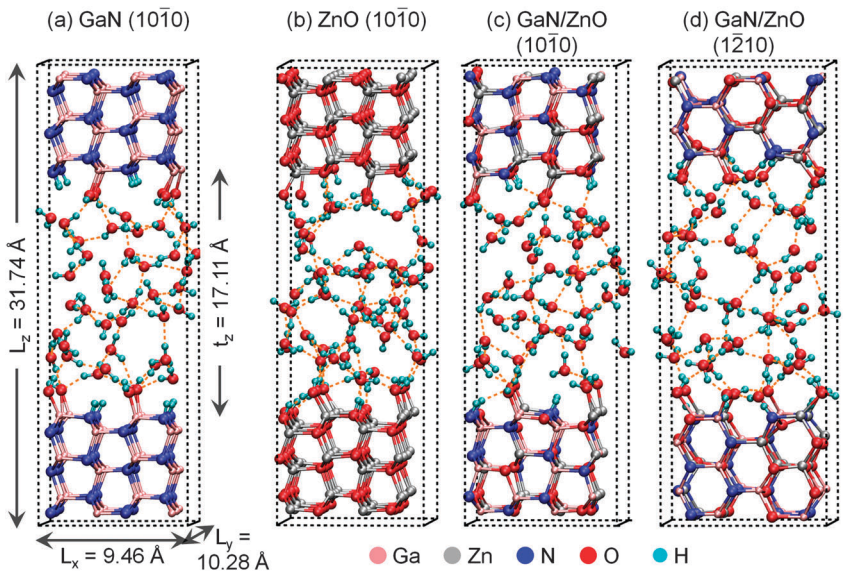

Fig. 3 Snapshots of equilibrated aqueous interfaces of (a) GaN$(10\bar{1}0)$, (b) ZnO$(10\bar{1}0)$, (c) GaN/ZnO$(10\bar{1}0)$, and (d) GaN/ZnO$(1\bar{2}10)$ surfaces.

Table 1 Dimensions of simulated cells

	Lateral dimensions (Å)		Thickness (Å)		
	L_x	L_y	L_z	t_z	# H_2O
GaN(10$\bar{1}$0)	9.46	10.28	31.74	17.11	48
ZnO(10$\bar{1}$0)	12.83	10.28	32.15	17.39	66
GaN/ZnO(10$\bar{1}$0)	9.56	10.33	31.22	16.42	48
GaN/ZnO(1$\bar{2}$10)	11.04	10.33	30.46	17.61	58

In terms of the primitive surface cells, the lateral dimensions of GaN(10$\bar{1}$0) and GaN/ZnO(10$\bar{1}$0) cells are 3 × 2, ZnO(10$\bar{1}$0) cells are 4 × 2, and GaN/ZnO(1$\bar{2}$10) cells are 2 × 2. Along the thickness direction all (10$\bar{1}$0) cells consist of 12 atomic layers while (1$\bar{2}$10) cell consists of 9 atomic layers.

between semiconductor surfaces is chosen such that the minimum distance between atoms in the semiconductor and water slabs is about 1 Å. We have performed BO DFT-MD simulations of each hydrated slab for 15 ps at 350 K using the simulation protocol described in Section 2.1.

3. Results and discussion

3.1 Interface equilibration

The starting configurations of our MD simulations consist of the clean semiconductor surfaces abruptly brought into contact with undissociated water molecules. As the simulations proceed, surface anion and cation sites promote the dissociation of water molecules into protons and hydroxide (OH^-) ions. The water dissociation is facilitated by the long-range attractive interactions between water molecules and surface anion and cation sites as evidenced by the fact that many water molecules dissociate before being adsorbed on the surface. The surface anions (N or O) act as bases accepting protons from dissociated water molecules while the corresponding OH^- ions bond with surface cations (Ga or Zn). The acid–base chemistry results in a hydroxylated surface, where the degree of hydroxylation varies with the surface composition and crystal orientation as discussed below.

The fractional occupancies of the surface anion and cation sites during MD runs are shown in Fig. 4 and 5. We used the following geometric criteria to obtain the statistical information on various types of species at the aqueous interface and in the bulk water region. The water molecules, OH^-, and H_3O^+ ions are identified based on the O–H bond distance cutoff of 1.2 Å. The surface N and O sites are considered protonated if the N–H and O–H bond lengths are less than 1.2 Å. Similarly, water molecules and OH^- are considered bonded to the semiconductor surface if the O-atom is within the cutoff radius of 2.5 Å from a surface cationic (Ga and Zn) site.

As seen in Fig. 4a, on the GaN(10$\bar{1}$0) surface the hydroxylation initially proceeds very rapidly such that about 70% of N sites become protonated within less than 0.5 ps. The hydroxylation then continues, albeit at a slower rate, until the surface is fully hydroxylated such that all N sites are protonated and all Ga atoms are bonded to OH^- ions. The full hydroxylation is in agreement with our earlier studies, which showed a negligible energy barrier for the dissociation of a water monolayer on the GaN(10$\bar{1}$0) surface.[55] An earlier DFT-MD study on the aqueous

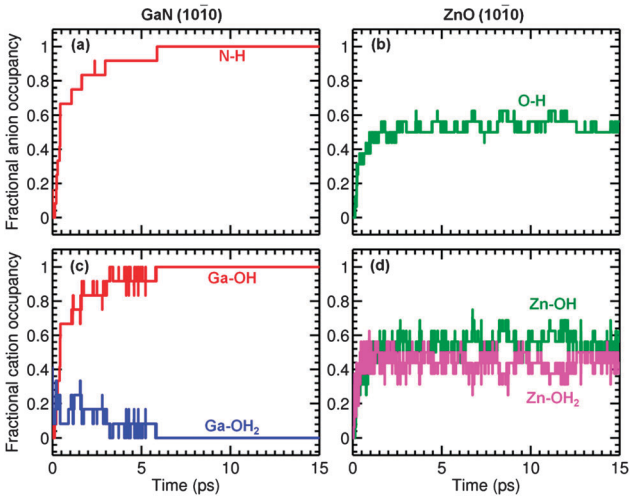

Fig. 4 Time dependence of fractional occupancy of surface anion (N and O) sites by protons and fractional occupancy of surface cation (Ga and Zn) sites by OH^- ions and water molecules. (a) N site occupancy on GaN(10$\bar{1}$0) surface. (b) O site occupancy on ZnO(10$\bar{1}$0) surface. (c) Ga site occupancy on GaN(10$\bar{1}$0) surface. (d) Zn site occupancy on ZnO(10$\bar{1}$0) surface.

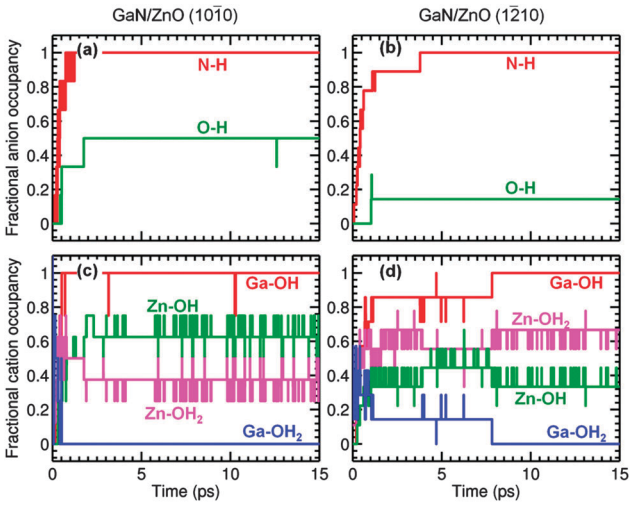

Fig. 5 Time dependence of fractional occupancy of anion (N and O) sites by protons on (a) GaN/ZnO(10$\bar{1}$0) and (b) GaN/ZnO(1$\bar{2}$10) surfaces. Time dependence of fractional occupancy of surface cation (Ga and Zn) sites by OH^- ions and water molecules on (c) GaN/ZnO(10$\bar{1}$0) and (d) GaN/ZnO(1$\bar{2}$10) surfaces.

GaN(10$\bar{1}$0) interface by Wang *et al.*[26] reported ≈83% hydroxylation on the GaN surface in contrast to the 100% hydroxylation found in our present DFT-MD study. However, further analysis by the same authors confirms that the 100% hydroxylated GaN(10$\bar{1}$0) surface is indeed more stable compared to the 83% hydroxylated GaN(10$\bar{1}$0) surface.[59]

The ZnO(10$\bar{1}$0) surface shows a very different hydroxylation behaviour compared to the GaN(10$\bar{1}$0) surface. About 50% of O sites become protonated within less than 1 ps (Fig. 4b). The population of protonated O sites then fluctuates between 50 and 62.5% for the remainder of the MD run. The corresponding OH^- ions are bonded to surface Zn atoms while the

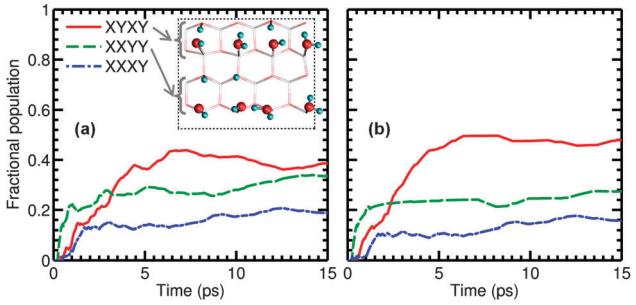

Fig. 6 Time-averaged fractional populations of various adsorption patterns of (a) OH^- ions and water molecules on Zn sites and (b) protons on O sites on the ZnO(10$\bar{1}$0) surface as a function of the simulation time. In (a), X corresponds to an OH^- ion adsorbed on a Zn site and Y corresponds to an intact water molecule adsorbed on a Zn site. In (b), X corresponds to a proton adsorbed on O site and Y corresponds to a free O site. Representative XYXY and XXYY patterns on Zn and O sites are schematically shown in the inset of (a).

remaining surface Zn atoms bond with intact water molecules (Fig. 4d). The degree of water dissociation in our MD simulations agrees well with earlier low temperature experimental and theoretical studies that found that in a water monolayer adsorbed on the ZnO(10$\bar{1}$0) surface, about 50% of the water molecules dissociate forming (2 × 1) structures.[56] Each (2 × 1) surface cell consists of a pair of alternating water molecules, one dissociated and one undissociated, resulting in repeated XY-structures along the [1$\bar{2}$10] direction.[56] Here, X corresponds to the Zn site bonded to an OH^- ion and Y corresponds to the Zn site bonded to an intact water molecule as illustrated in the inset of Fig. 6a. Fig. 6a shows the time-averaged populations of various water dissociation patterns along [1$\bar{2}$10] directed Zn rows obtained from MD simulations. The repeated XY-structures, similar to those observed in experiments, are also obtained in our MD simulations. However, our MD simulations also exhibit XXYY- and XXXY structures along Zn rows. Since the X motif corresponds to local dissociation of water, the overall pattern can also be probed by looking at the population of protons adsorbed on O sites along the [1$\bar{2}$10] direction. Indeed, these exhibit a strongly correlated pattern (Fig. 6b), although the quantitative relative populations are slightly different.

Next, we consider the more complex non-polar (10$\bar{1}$0) and (1$\bar{2}$10) surfaces of the GaN/ZnO alloy. Including the top and bottom surfaces, the model supercell of the GaN/ZnO(10$\bar{1}$0)–water interface (Fig. 3c) contains 4 Ga, 8 Zn, 6 N, and 6 O surface sites. Similarly, there are 7 Ga, 9 Zn, 9 N, and 7 O surface sites in the model supercell of the GaN/ZnO(1$\bar{2}$10)–water interface (Fig. 3d). We find 75% and 62.5% hydroxylation on (10$\bar{1}$0) and (1$\bar{2}$10) surfaces, respectively. To determine qualitatively the relative acidity and basicity of different surface sites, we plot their fractional occupancies as a function of the simulation time in Fig. 5. As seen in Fig. 5a and b, all N sites are protonated on both surfaces, while only 50% and 14.3% of O sites are protonated on (10$\bar{1}$0) and (1$\bar{2}$10) surfaces, respectively. This indicates that N sites show stronger basic character compared to O sites. Moreover, O sites on the (10$\bar{1}$0) surface are stronger bases compared to O sites on the (1$\bar{2}$10) surface. Among the cationic sites, Ga sites show stronger affinity for OH^- ions indicating their stronger acidic character compared to that of Zn sites (Fig. 5c and d). Zn sites on the (10$\bar{1}$0) surface appear to have stronger affinity for OH^- ions compared to those on the (1$\bar{2}$10) surface. However, the very different relative proportion of cationic sites (Zn *vs.* Ga sites) on our (10$\bar{1}$0) and (1$\bar{2}$10) model surfaces prevents any definitive comparison of the acidities of Zn sites on (10$\bar{1}$0) and (1$\bar{2}$10) surfaces.

We analyzed the RDFs to compare the bond lengths of various Cat–O_w type bonds, where 'Cat' is a cationic site on the semiconductor surface and 'O_w' is an oxygen atom in an OH^- ion or an intact water molecule. The RDFs obtained from the equilibrated MD trajectories with duration from 10 to 15 ps are shown in Fig. S4 in the ESI.† The Cat–O_w bond lengths vary within the range of 1.5–2.3 Å such that $l_{GaOH} < l_{ZnOH} < l_{ZnOH_2}$, where l is the bond length.

3.2 Proton dynamics

In this section, we use occupancies of the surface anion and cation sites by the protons, OH^- ions and water molecules (Fig. 4 and 5) to deduce qualitative features of the surface-dependent proton dynamics, but defer their detailed quantitative analysis for future work. We consider the MD simulation trajectories beyond 6 ps, where all surfaces have reached a steady-state in terms of protonation of surface anions. The population of the protonated anions on the (10$\bar{1}$0) surface of pure GaN and the (10$\bar{1}$0) and (1$\bar{2}$10) surfaces of the 1 : 1 GaN/ZnO alloy is static, indicating that anionic sites do not participate in proton transfer processes on time scales less than 10 ps. On the ZnO(10$\bar{1}$0) surface, however, the population of the protonated anions (O atoms) fluctuates between 50 to 62.5%. These fluctuations originate from the dynamic dissociation/association of water molecules adsorbed on the surface Zn sites. The proton transfer mechanism corresponding to such dissociation/association events is illustrated in Fig. 7a. In the dissociation event, a proton donated by an adsorbed water molecule protonates a nearby surface O site. While in the association event, a proton donated by a surface O site recombines with the OH^- ion bonded to a nearby Zn site. Similar dissociation/association dynamics have been observed in the combined experimental and computational studies on a water monolayer adsorbed on a ZnO(10$\bar{1}$0) surface.[56] Our first-principles MD simulations show that these dissociation/association processes are also present on the fully solvated ZnO(10$\bar{1}$0) surface under ambient conditions, and they take place on a picosecond time scale.

The populations of the OH^- ions and water molecules adsorbed on surface Zn sites also exhibit fluctuations. These fluctuations

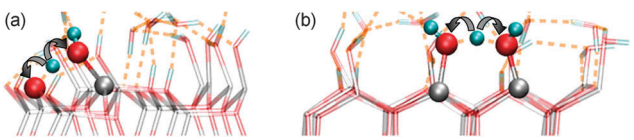

Fig. 7 Schematic of proton transfer (a) between an O site and a water molecule adsorbed on the nearby Zn site and (b) between an OH^- ion and a water molecule adsorbed on adjacent Zn sites.

originate from proton transfer between surface-bound species and from proton transfer between a surface-bound species and a water molecule in the solvent region. As illustrated in Fig. 7, the proton transfer processes between surface-bound species can be classified in two types: (i) proton transfer between an O site and a water molecule adsorbed on a nearby Zn site, which occurs only on the ZnO surface, and (ii) proton transfer between an OH^- ion and a water molecule adsorbed on adjacent Zn sites, which occurs on ZnO and GaN/ZnO alloy surfaces. Additionally, these fluctuations also include signatures of thermal variations in the O–H bond length in the adsorbed OH^- ions and water molecules because we have used a fixed O–H bond distance cutoff of 1.2 Å to distinguish between OH^- ions and water molecules. Our future studies will include detailed quantitative analysis of various dynamical proton transfer processes on these surfaces.

3.3 Thickness of interfacial layer

In this section, we investigate the structure of water as a function of the distance from the semiconductor surface using MD trajectories with duration from 10 to 15 ps for each of the four surfaces. Results for the GaN/ZnO($10\bar{1}0$) surface are summarized in Fig. 8 while results for the other three surfaces are provided in Fig. S5–S7 in the ESI.† Fig. 8a shows the planar averaged density of water molecules and OH^- ions for the GaN/ZnO($10\bar{1}0$)–water interface. The OH^- ions are strongly bound to the surface cations as indicated by the sharp peaks in the density of OH^- ions close to the semiconductor surfaces. The surface-bound water molecules give rise to a shoulder in the density of water molecules close to the semiconductor surfaces.

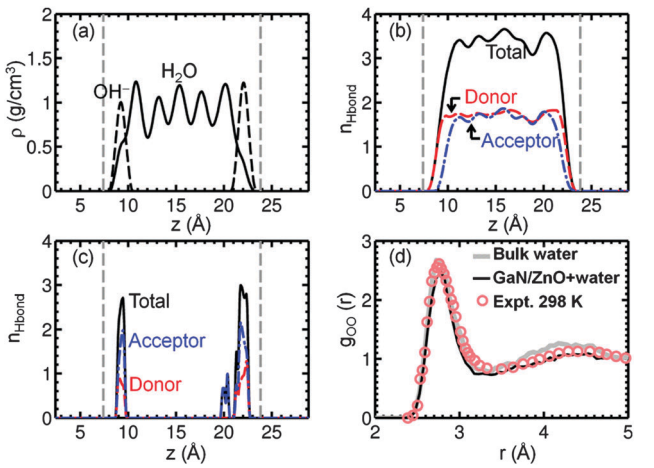

Fig. 8 Structure of water as a function of distance from the GaN/ZnO($10\bar{1}0$) surface. (a) Planar and time averaged density of water molecules and OH^- ions. Average number of donor (dashed line), acceptor (dash-dotted line) and total (solid line) hydrogen bonds per (b) water molecule and (c) OH^- ion. The vertical dashed lines in (a–c) indicate the nominal positions of the top and bottom semiconductor surfaces. (d) Oxygen–oxygen radial distribution function (RDF) calculated from a water layer consisting of water molecules more than 3 Å away from the semiconductor surface in GaN/ZnO–water interface simulation (dark line) along with the calculated (faint line) and experimentally derived (hollow circles) RDFs of bulk water. The RDFs of bulk water are the same as in Fig. 2.

Beyond the surface-bound layer, the density of water molecules shows an oscillatory behaviour resulting from the layering effect caused by the ''hard-wall'' boundary conditions at the semiconductor surface. The other three surfaces also show similar variations in the density of water molecules and OH^- ions (Fig. S5a, S6a, and S7a, ESI†). Owing to its more corrugated structure, the GaN/ZnO($1\bar{2}10$) surface induces much stronger oscillations in the density of water. This type of layering effect has been reported for several other surfaces, *e.g.*, experimental studies on the aqueous interface of a mica surface and theoretical studies on aqueous interfaces of SiC,[24] NaCl,[60] InP, and GaP,[25] *etc.*

In order to gain further insight into the structure of water, we examine the hydrogen bond network of water molecules (Fig. 8b) and OH^- ions (Fig. 8c). The hydrogen bonds are defined using the same criteria as used for the bulk water simulations described in Section 2.3. The adsorbed water molecules mostly form donor hydrogen bonds with bulk water as evidenced by the fact that, close to the semiconductor surface, the number of donor hydrogen bonds dominates over the number of acceptor hydrogen bonds (Fig. 8b). The bulk-water-like hydrogen bond network characterized by an equal number of donor and acceptor hydrogen bonds is recovered beyond a 3 Å distance from the surface. In this bulk water or solvent region, the average number of hydrogen bonds per water molecule is 3.46, which is in close agreement with the value of 3.54 in our bulk water simulations using a 32 water molecule cell. The surface bound OH^- ions form both donor and acceptor hydrogen bonds with the water molecules in the solvent region and with the OH^- ions and water molecules adsorbed on nearby cationic sites (Fig. 8c). The number of acceptor hydrogen bonds is higher than the number of donor hydrogen bonds. A secondary peak around 20 Å in Fig. 8c arises from the OH^- ions created during proton exchange events between a surface-bound species and a water molecule in the solvent region. Such OH^- ions have a very short lifetime, and as a result there is no corresponding peak in the planar and time-averaged density of OH^- ions in Fig. 8a. The hydrogen bond networks at the aqueous interfaces of the other three surfaces (Fig. S5–S7, ESI†) are also found to exhibit similar characteristics.

Fig. 8d shows the oxygen–oxygen RDF, $g_{OO}(r)$ of water molecules more than 3 Å away from the GaN/ZnO($10\bar{1}0$) surface. The $g_{OO}(r)$ of this thin water layer is calculated using a modified normalization scheme proposed by Kaya *et al.*[61] and it is found to compare well with the experimental $g_{OO}(r)$ and that computed using our bulk water simulations using a 32 water molecule cell. The other three surfaces are also found to show a very similar $g_{OO}(r)$ as shown in Fig. S5d, S6d, and S7d in the ESI.† Thus the structural analysis of all four semiconductor surfaces suggests that the aqueous interface chemistry significantly alters the structure of water within 3 Å distance from the surface. The oscillations in the density of water induced by the semiconductor surface persist through the entire thickness of the water layer indicating that such oscillations extend to longer length scales compared to those included in the simulation domain. In spite of the density oscillations, the structure of the water layer beyond 3 Å distance from the semiconductor surface is very similar to that of

bulk water in terms of the hydrogen bond network and the oxygen–oxygen radial distribution function.

3.4 Electronic structure

Our earlier mechanistic studies of water oxidation at the GaN(10$\bar{1}$0)–water interface showed that the water oxidation process is driven by the localization of the photogenerated holes on the OH^- ions adsorbed on the Ga sites.[7] Water oxidation on ZnO and GaN/ZnO alloy surfaces is expected to follow a similar mechanism. To this end, we analyze the propensity of localization of the photogenerated holes on surface OH^- ions by means of the projected density of states (PDOS). Fig. 9 shows the PDOS for various atomic species at the (10$\bar{1}$0) surface of GaN, ZnO, and the 1 : 1 GaN/ZnO alloy obtained by averaging the results from 50 snapshots randomly selected from MD trajectories over a period of 10 to 15 ps. To probe the local electronic structure and avoid averaging over the potential difference arising from the asymmetric surface dipoles caused by the different degree of surface hydroxylation, the PDOS is averaged over only one of the two (top or bottom) semiconductor surfaces. The energy levels are aligned with the valence band edge of the respective bulk material using the average electrostatic potential as a common reference. The valence band edge of the bulk material is obtained from a MD simulation using the same semiconductor slab from the aqueous interface simulation but with full periodic boundary conditions.

Fig. 9a shows that near the valence band edge, states from the GaN(10$\bar{1}$0)–water interface have a significant contribution from the protonated N atoms and O atoms of the OH^- ions adsorbed on Ga sites, with the latter more prominent. A thermal population of holes would have somewhat more weight on the surface OH^- ions. At the ZnO(10$\bar{1}$0)–water interface, however, the density of states on the non-protonated O atoms that are available due to partial interface water dissociation falls higher in energy than that on the Zn-bound OH^- (Fig. 9b). Relative to the bulk valence band edge, this suggests trapping of holes on the non-protonated O atoms, with activation needed to place holes in the OH^-. The O sites with protons passivating the dangling bonds on the surface have a similar density of states to the protonated N atoms in the GaN case (Fig. 9a). At the GaN/ZnO(10$\bar{1}$0)–water interface, the density of states associated with the GaOH and the ZnOH are systematically pushed lower in energy. As a consequence, the holes are most likely to localize on either the protonated N atoms or the non-protonated O atoms with the latter having higher density of states per site (Fig. 9d). This PDOS analysis suggests that the GaN(10$\bar{1}$0) surface should oxidize water more efficiently on a per-generated-hole basis compared to the ZnO and GaN/ZnO(10$\bar{1}$0) surfaces. However, future work will be needed in order to probe hole localization and the response of the interface structure.

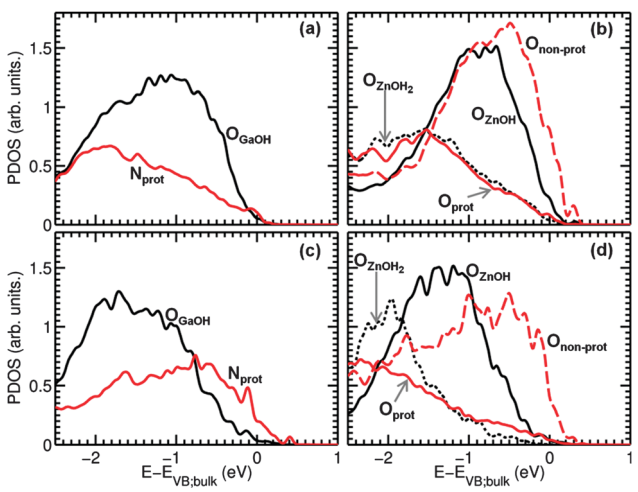

Fig. 9 Projected density of states (PDOS) for various atomic species at the aqueous interfaces of the (10$\bar{1}$0) surfaces of GaN, ZnO, and GaN/ZnO alloy. (a) GaN surface, (b) ZnO surface, (c) "GaN like" surface species on GaN/ZnO surface, and (d) "ZnO like" surface species on GaN/ZnO surface. The labels are explained as follows. N_{prot}: protonated N site. O_{prot}: protonated O site. $O_{non\text{-}prot}$: non-protonated O site. O_{GaOH}: O in OH^- ion adsorbed on Ga site. O_{ZnOH}: O in OH^- ion adsorbed on Zn site. O_{ZnOH_2}: O in intact water molecule adsorbed on Zn site.

4. Conclusions and future directions

To summarize, using first-principles DFT-MD, we have analyzed the structure of aqueous interfaces of the non-polar wurtzite facets of GaN, ZnO, and the 1 : 1 GaN/ZnO alloy. Specifically, the (10$\bar{1}$0) surface of GaN, ZnO, and the 1 : 1 GaN/ZnO alloy as well as the (1$\bar{2}$10) surface of 1 : 1 GaN/ZnO alloy are studied. We find that water adsorption on all these surfaces is substantially dissociative. The surface anions act as bases accepting protons from dissociated water molecules while the corresponding OH^- ions bond with surface cations. Surface N sites show stronger basic character and are protonated more readily than surface O sites. All surface Ga sites are bonded to OH^- ions while surface Zn sites are bonded either to OH^- ions or intact water molecules. The strong perturbation in the water structure, induced by the acid–base chemistry at the solvated surface, extends up to 3 Å distance from the surface. Additionally, the semiconductor surface induces oscillations in the density of water. The water layer beyond 3 Å distance from the semiconductor surface exhibits a bulk-like hydrogen bond network and oxygen–oxygen radial distribution function. The electronic structure analysis of (10$\bar{1}$0) surfaces shows that the valence energy levels of the adsorbed OH^- ions are located below the valence energy levels of some other surface species (particularly protonated N and non-protonated O atoms). This indicates that the photogenerated holes may become trapped by surface species other than the adsorbed OH^- ions; consequently, the water oxidation process may involve reaction barriers related to hole transfer from those surface species to adsorbed OH^- ions.

The present work sets the stage for the following further studies on the aqueous interfaces of the GaN/ZnO alloy. (i) *Redox level alignment*: the fact that the bulk-like structure of water is recovered beyond a 3 Å distance from the semiconductor surface indicates that there is a sufficiently thick (about 10 Å) bulk water layer to permit the structural and electronic properties of water to be well converged in the MD simulations presented here.

We have developed a method based on first-principles MD to calculate the redox level alignment at the aqueous semiconductor interface and have applied it to the $(10\bar{1}0)$ surfaces of pure GaN and ZnO.[32] Our future work will involve applying the newly developed method along with the MD simulations presented here to compute the redox level alignment at the aqueous interfaces of GaN/ZnO surfaces. (ii) *Mechanistic studies of water oxidation*: for the mechanistic studies of water oxidation at the aqueous GaN/ZnO interfaces, we will use the approach combining first-principles MD and cluster models that was employed in our earlier work on water oxidation at the aqueous GaN$(10\bar{1}0)$ interface.[7] The structural models of the catalytic sites will be obtained from the MD simulations presented here. (iii) *Proton dynamics*: as described in Section 3.2, the MD simulations show signatures of interesting surface-dependent proton dynamics. Our future work will involve quantitative analysis of various proton transfer processes and calculation of relative acidity and basicity of various surface sites to determine the stability of those surface sites under varying pH conditions.

Acknowledgements

We thank P. B. Allen and M. Fernandez-Serra for valuable discussions. This work was carried out at Brookhaven National Laboratory under contract No. DE-AC02-98CH10886 with the U.S. Department of Energy and supported by its Office of Basic Energy Sciences, its Division of Chemical Sciences, its Computational Materials and Chemical Sciences Network program, and its Scientific User Facilities Division. This research utilized resources at the Center for Functional Nanomaterials at Brookhaven National Laboratory and the National Energy Research Scientific Computing Center at Lawrence Berkeley National Laboratory, which is supported by the Office of Science of the U.S. Department of Energy under Contract No. DE-AC02-05CH11231.

Notes and references

1 N. S. Lewis and D. G. Nocera, *Proc. Natl. Acad. Sci. U. S. A.*, 2006, **103**, 15729–15735.
2 K. Maeda, K. Teramura, N. Saito, Y. Inoue and K. Domen, *Bull. Chem. Soc. Jpn.*, 2007, **80**, 1004–1010.
3 D. F. Wang, A. Pierre, M. G. Kibria, K. Cui, X. G. Han, K. H. Bevan, H. Guo, S. Paradis, A. R. Hakima and Z. T. Mi, *Nano Lett.*, 2011, **11**, 2353–2357.
4 K. Maeda, K. Teramura, D. L. Lu, T. Takata, N. Saito, Y. Inoue and K. Domen, *Nature*, 2006, **440**, 295.
5 J. Cheng and M. Sprik, *Phys. Chem. Chem. Phys.*, 2012, **14**, 11245–11267.
6 J. K. Norskov, T. Bligaard, J. Rossmeisl and C. H. Christensen, *Nat. Chem.*, 2009, **1**, 37–46.
7 X. A. Shen, Y. A. Small, J. Wang, P. B. Allen, M. V. Fernandez-Serra, M. S. Hybertsen and J. T. Muckerman, *J. Phys. Chem. C*, 2010, **114**, 13695–13704.
8 A. Xiong, T. Yoshinaga, T. Ikeda, M. Takashima, T. Hisatomi, K. Maeda, T. Setoyama, T. Teranishi and K. Domen, *Eur. J. Inorg. Chem.*, 2014, 767–772.
9 L. L. Jensen, J. T. Muckerman and M. D. Newton, *J. Phys. Chem. C*, 2008, **112**, 3439–3446.
10 L. Li, J. T. Muckerman, M. S. Hybertsen and P. B. Allen, *Phys. Rev. B: Condens. Matter Mater. Phys.*, 2011, **83**, 134202.
11 S. Z. Wang and L. W. Wang, *Phys. Rev. Lett.*, 2010, **104**, 065501.
12 C. Di Valentin, *J. Phys. Chem. C*, 2010, **114**, 7054–7062.
13 M. N. Huda, Y. F. Yan, S. H. Wei and M. M. Al-Jassim, *Phys. Rev. B: Condens. Matter Mater. Phys.*, 2008, **78**, 195204.
14 W. Wei, Y. Dai, K. S. Yang, M. Guo and B. B. Huang, *J. Phys. Chem. C*, 2008, **112**, 15915–15919.
15 H. Chen, W. Wen, Q. Wang, J. C. Hanson, J. T. Muckerman, E. Fujita, A. I. Frenkel and J. A. Rodriguez, *J. Phys. Chem. C*, 2009, **113**, 3650–3659.
16 H. Y. Chen, L. P. Wang, J. M. Bai, J. C. Hanson, J. B. Warren, J. T. Muckerman, E. Fujita and J. A. Rodriguez, *J. Phys. Chem. C*, 2010, **114**, 1809–1814.
17 E. J. McDermott, E. Z. Kurmaev, T. D. Boyko, L. D. Finkelstein, R. J. Green, K. Maeda, K. Domen and A. Moewes, *J. Phys. Chem. C*, 2012, **116**, 7694–7700.
18 A. A. Reinert, C. Payne, L. M. Wang, J. Ciston, Y. M. Zhu and P. G. Khalifah, *Inorg. Chem.*, 2013, **52**, 8389–8398.
19 K. Lee, B. M. Tienes, M. B. Wilker, K. J. Schnitzenbaumer and G. Dukovic, *Nano Lett.*, 2012, **12**, 3268–3272.
20 J. Liu, L. S. Pedroza, C. Misch, M. V. Fernández-Serra and P. B. Allen, *J. Phys.: Condens. Matter*, 2014, in press.
21 S. H. Wei, L. G. Ferreira, J. E. Bernard and A. Zunger, *Phys. Rev. B: Condens. Matter Mater. Phys.*, 1990, **42**, 9622–9649.
22 H. Cheng and A. Selloni, *Langmuir*, 2010, **26**, 11518–11525.
23 J. Cheng and M. Sprik, *Phys. Rev. B: Condens. Matter Mater. Phys.*, 2010, **82**, 081406.
24 G. Cicero, J. C. Grossman, A. Catellani and G. Galli, *J. Am. Chem. Soc.*, 2005, **127**, 6830–6835.
25 B. C. Wood, E. Schwegler, W. I. Choi and T. Ogitsu, *J. Am. Chem. Soc.*, 2013, **135**, 15774–15783.
26 J. Wang, L. S. Pedroza, A. Poissier and M. V. Fernandez-Serra, *J. Phys. Chem. C*, 2012, **116**, 14382–14389.
27 G. Tocci and A. Michaelides, *J. Phys. Chem. Lett.*, 2014, **5**, 474–480.
28 J. Rossmeisl, Z. W. Qu, H. Zhu, G. J. Kroes and J. K. Norskov, *J. Electroanal. Chem.*, 2007, **607**, 83–89.
29 A. Valdes, Z. W. Qu, G. J. Kroes, J. Rossmeisl and J. K. Norskov, *J. Phys. Chem. C*, 2008, **112**, 9872–9879.
30 A. Valdes and G. J. Kroes, *J. Chem. Phys.*, 2009, **130**, 114701.
31 A. Valdes and G. J. Kroes, *J. Phys. Chem. C*, 2010, **114**, 1701–1708.
32 N. Kharche, J. T. Muckerman and M. S. Hybertsen, 2014, unpublished.
33 A. V. Akimov, J. T. Muckerman and O. V. Prezhdo, *J. Am. Chem. Soc.*, 2013, **135**, 8682–8691.
34 G. Kresse and J. Furthmuller, *Phys. Rev. B: Condens. Matter Mater. Phys.*, 1996, **54**, 11169–11186.
35 G. Kresse and D. Joubert, *Phys. Rev. B: Condens. Matter Mater. Phys.*, 1999, **59**, 1758–1775.

36 See http://www.vasp.at/ for the computational software.
37 P. E. Blochl, *Phys. Rev. B: Condens. Matter Mater. Phys.*, 1994, **50**, 17953–17979.
38 S. L. Dudarev, G. A. Botton, S. Y. Savrasov, C. J. Humphreys and A. P. Sutton, *Phys. Rev. B: Condens. Matter Mater. Phys.*, 1998, **57**, 1505–1509.
39 M. Dion, H. Rydberg, E. Schroder, D. C. Langreth and B. I. Lundqvist, *Phys. Rev. Lett.*, 2004, **92**, 246401.
40 J. Wang, G. Roman-Perez, J. M. Soler, E. Artacho and M. V. Fernandez-Serra, *J. Chem. Phys.*, 2011, **134**, 024516.
41 C. Zhang, J. Wu, G. Galli and F. Gygi, *J. Chem. Theory Comput.*, 2011, **7**, 3054–3061.
42 A. Mogelhoj, A. K. Kelkkanen, K. T. Wikfedt, J. Schiotz, J. J. Mortensen, L. G. M. Pettersson, B. I. Lundqvist, K. W. Jacobsen, A. Nilsson and J. K. Norskov, *J. Phys. Chem. B*, 2011, **115**, 14149–14160.
43 I. C. Lin, A. P. Seitsonen, I. Tavernelli and U. Rothlisberger, *J. Chem. Theory Comput.*, 2012, **8**, 3902–3910.
44 J. P. Perdew, K. Burke and M. Ernzerhof, *Phys. Rev. Lett.*, 1996, **77**, 3865–3868.
45 J. Klimes, D. R. Bowler and A. Michaelides, *J. Phys.: Condens. Matter*, 2010, **22**, 022201.
46 See http://www.gromacs.org/ for the computational software.
47 See http://www.gaussian.com/g_prod/g09.htm for the computational software.
48 T. Helgaker, W. Klopper, H. Koch and J. Noga, *J. Chem. Phys.*, 1997, **106**, 9639–9646.
49 E. Schwegler, J. C. Grossman, F. Gygi and G. Galli, *J. Chem. Phys.*, 2004, **121**, 5400–5409.
50 P. H. L. Sit and N. Marzari, *J. Chem. Phys.*, 2005, **122**, 204510.
51 A. K. Soper and C. J. Benmore, *Phys. Rev. Lett.*, 2008, **101**, 065502.
52 M. V. Fernandez-Serra and E. Artacho, *J. Chem. Phys.*, 2004, **121**, 11136–11144.
53 I. C. Yeh and G. Hummer, *J. Phys. Chem. B*, 2004, **108**, 15873–15879.
54 B. Dunweg and K. Kremer, *J. Chem. Phys.*, 1993, **99**, 6983–6997.
55 X. Shen, P. B. Allen, M. S. Hybertsen and J. T. Muckerman, *J. Phys. Chem. C*, 2009, **113**, 3365–3368.
56 O. Dulub, B. Meyer and U. Diebold, *Phys. Rev. Lett.*, 2005, **95**, 136101.
57 J. E. Northrup and J. Neugebauer, *Phys. Rev. B: Condens. Matter Mater. Phys.*, 1996, **53**, 10477–10480.
58 D. J. Cooke, A. Marmier and S. C. Parker, *J. Phys. Chem. B*, 2006, **110**, 7985–7991.
59 J. Liu, M. V. Fernandez-Serra and P. B. Allen, Stony Brook University, Stony Brook, NY, Private Communication, 2013.
60 L. Liu, M. Krack and A. Michaelides, *J. Am. Chem. Soc.*, 2008, **130**, 8572–8573.
61 S. Kaya, D. Schlesinger, S. Yamamoto, J. T. Newberg, H. Bluhm, H. Ogasawara, T. Kendelewicz, G. E. Brown, L. G. M. Pettersson and A. Nilsson, *Sci. Rep.*, 2013, **3**, 1074.

